Journal of Colloid and Interface Science 356 (2011) 369–372

Contents lists available at ScienceDirect

Journal of Colloid and Interface Science

www.elsevier.com/locate/jcis

Short communication

Microemulsion-mediated sol–gel synthesis of mesoporous rutile TiO_2 nanoneedles and its performance as anode material for Li-ion batteries

Ramdas B. Khomane *

CSIR – Central Electrochemical Research Institute, CECRI – Madras Unit, CSIR Madras Complex, Taramani, Chennai 600 113, India

ARTICLE INFO

Article history:
Received 22 September 2010
Accepted 16 December 2010
Available online 19 December 2010

Keywords:
Microemulsion
Sol–gel
Mesoporous
TiO_2 nanoneedles
Discharge capacity

ABSTRACT

Mesoporous rutile TiO_2 nanoneedles have been successfully synthesized using a reverse microemulsion-mediated sol–gel method at room temperature. The materials were characterized by X-ray diffraction (XRD), transmission electron microscopy (TEM), and the Bruauner–Emmet–Teller (BET) adsorption method, and their electrochemical properties were investigated by galvanostatic charge and discharge tests. XRD observations revealed the formation of a pure rutile TiO_2 phase. Furthermore, TEM observation revealed the presence of a highly porous needle-like morphology. The electrochemical measurements show that the nanoneedles deliver an initial capacity of 305 mA h g^{-1} as anode material for Li-ion batteries and sustain a capacity value of 128 mA h g^{-1} beyond 15 cycles. The reported synthesis is simple, mild, energy efficient, and without postcalcination.

1. Introduction

Recently, considerably attention has been paid to the synthesis of one-dimensional (1D) nanostructures such as nanorods, nanoneedles, nanotubes, and nanowires due to their potential applications in fabrication of nanoscale electronic devices [1]. These 1D nanoscale structures are essentially single crystals, free from any lattice defects, and form as a result of anisotropic crystal growth in the reaction media [2]. Therefore, various methods such as electron beam lithography [3], chemical vapor deposition [4], surfactant-directed synthesis [5], reverse microemulsion [6], hydrothermal synthesis [7], solvothermal [8], and filling of templates with colloidal oxide particles [9] have been developed for the preparation of 1D nanostructures. Among these, the method of reverse microemulsion for the synthesis of 1D nanostructures was regarded as a very facile and efficient route. In reverse microemulsion, aqueous solution disperses in the organic phase and forms a number of nanometer-scale droplets. These droplets not only act as a nanoreactor in the reaction process but also inhibit the aggregation of nanoparticles. The principal advantage of using reverse microemulsion is that particle shape and corresponding size distributions can be readily controlled by adjusting the molar ratio of water to surfactant, aging time, and reactant concentration.

Titanium dioxide is one of the most important and widely used metal oxides for technological applications, including, e.g., photocatalysis [10], rechargeable lithium ion batteries [11], solar energy conversion [12], and gas sensors [13]. TiO_2 exists in four polymorphic forms: anatase (tetragonal, space group I41/amd), rutile (tetragonal, space group P42/mnm), brookite (orthorhombic, space group Pbca), and TiO_2 (B) (monoclinic, space group C2/m). The nanostructured TiO_2 exhibits better lithium ion transfer due to a better electrolyte/material interaction compared with the bulk nonporous material. It is well known that lithium insertion into bulk rutile is negligible at room temperature [14] but it can be reversibly inserted into nanometer-sized rutile [15]. Therefore, control of the morphology of rutile TiO_2 nanomaterials using soft templates at room temperature is very important for achieving a better electrochemical performance. Additionally, a room temperature approach also saves energy consumed in the preparation steps and reducing the overall cost.

In this study, mesoporous rutile nanoneedles were prepared in Triton X-100-based water-in-oil reverse microemulsion at room temperature. The morphological features of the nanoneedles were investigated by TEM and the electrochemical properties of these nanoneedles as anode materials for lithium ion batteries were also discussed.

2. Experimental procedure

2.1. Chemicals and materials

Titanium isopropoxide was purchased from Aldrich and Triton X-100 [polyoxyethylene (10) octylphenyl ether] was purchased from Acros Organics. Organic solvents such as cyclohexaneand *n*-hexanol used were analytical grade and obtained from various sources.

* Fax: +91 44 2254 2456.
E-mail address: ramdasbk@yahoo.com

0021-9797/$ - see front matter © 2010 Elsevier Inc. All rights reserved.
doi:10.1016/j.jcis.2010.12.048

2.2. Synthesis of TiO_2 nanoneedles

Rutile TiO_2 nanoneedles were synthesized by direct addition of titanium isopropoxide to reverse microemulsion of Triton X-100/cyclohexane/*n*-hexanol/water. Reverse microemulsion solution was prepared using 52 wt.% cyclohexane as the oil phase, 22 wt.% Triton X-100 as a surfactant, 11 wt.% *n*-hexanol as cosurfactant (surfactant:cosurfactant ratio of 2:1 by weight), and 15 wt.% aqueous phase. The amount of 66 g of Triton X-100 with 33 g of *n*-hexanol was added to 156 g of cyclohexane and 5 ml of 37% HCl was mixed with 40 ml of Millipore water which can be used as an aqueous phase in reverse microemulsion. This microemulsion was stirred for 10 min at room temperature to obtain an optically clear and stable reverse microemulsion. To this reverse microemulsion solution 8.52 g of titanium isopropoxide was added slowly under vigorous stirring. In this step titanium isopropoxide was gradually hydrolyzed and condensed in water droplets. The resulting solution was stirred for 24 h to obtain a fine suspension of the product and aged for 24 h. The suspension was recovered by centrifugation and washed thoroughly by ethanol, acetone, and deionized water and then oven dried at 110 °C for 12 h.

Phase identification was carried out by X-ray powder diffraction XRD 3003TT (GE Inspection Technologies) diffractometer with Cu Kα (1.54 Å) radiation. The diffraction patterns were recorded in the 20–70° range. The morphology of the TiO_2 was observed by transmission electron microscope. The electrochemical evaluation of the TiO_2 anode materials was accomplished by assembling a Swagelok-type cell. The working electrodes were made by mixing 85% active material with 15% SP carbon, which acts as the electrical conductor. The cells were assembled and sealed in an argon-filled glove box with lithium metal as a counter- and reference-electrode. The electrolyte was 1 M $LiPF_6$ dissolved in EC/DMC with a volume ratio of 1:1. The glass fiber separator soaked with electrolyte was put between the electrolytes. The cells thus fabricated were cycled galvanostatically in the voltage range between 1 and 3 V versus lithium using a VMP3Z multichannel potentiostat/galvanostat.

3. Results and discussion

3.1. X-ray diffraction study

Powder X-ray diffraction measurements were performed using Cu Kα radiation (λ = 1.5418 Å) on a GE 3003TT with 2θ in the range from 20° to 70° at a scan rate of 4°/min. The XRD pattern of the as-prepared sample (Fig. 1) exhibits diffraction peaks at 2θ of 27.4°, 36°, 41.2°, 44°, 54.27°, and 56.6° which can be readily indexed to the rutile phase of TiO_2 (JCPDS No. 21-1276). No other peaks corresponding to the anatase or brookite phases were observed, indicating the high purity of the product. The presence of a well-defined diffraction pattern with high-intensity peaks suggests that the as-synthesized product was highly crystallized. Also, all peaks were broad, which was indicative of the formation of small crystallites by microemulsion-coupled sol–gel techniques.

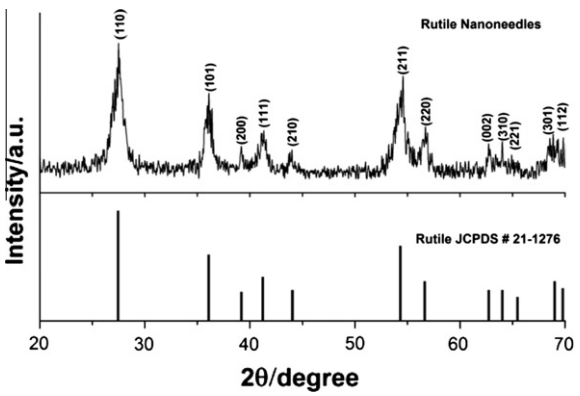

Fig. 1. X-ray diffraction pattern of mesoporous rutile TiO_2 nanoneedles.

3.2. TEM study

Transmission electron microscopy (TEM) was employed to observe the morphology of the as-prepared rutile TiO_2 sample. The TEM image (Fig. 2A) shows the presence of needle-like highly developed nanocrystalline rutile TiO_2 with a width of 20–25 nm and length of >100 nm. It is observed by TEM that the rutile TiO_2 crystal aligned in a specific crystallographic direction forming mesoporous needle-like aggregates (Fig. 2B). Selected area electron diffraction (SAED) patterns (inset in 2A) clearly indicate the highly crystalline nature of the sample. The SAED patterns also show a pair of strong (1 1 0) reflections, indicating that the (1 1 0) planes of the rutile nanocrystals are locally preferably oriented. It is evident from TEM images that the nanoneedle morphology is retained despite the creation of porosities arising from the removal of water and surfactant molecules. This observation was further proved by nitrogen isothermal adsorption–desorption techniques (Fig. 3).

3.3. N_2 adsorption–desorption study

The isotherm represents a pore structure of type IV [8], which is typical for mesoporous materials with a hysteresis loop of type H3, according to the definition of IUPAC [9]. The hysteresis loop was at relative pressures between 0.55 and 1.0 which may represent interparticle pores within the samples. The Barrett–Joyner–Halenda (BJH) pore-size distribution [16] is shown in the inset of Fig. 3. The mesopore-size distribution is in the range of 3–19 nm with an average pore diameter of 10 nm. The results are well in agreement with TEM characterization. According to Brunauer–Emmett–Teller (BET) analysis, a total specific surface area and pore volume of the mesoporous TiO_2 are 135 $m^2\ g^{-1}$ and 0.572 $cm^3\ g^{-1}$, respectively.

3.4. Electrochemical study

The lithium insertion/deinsertion reaction into the rutile TiO_2 can be written as $TiO_2 + xLi^+ + xe^- \leftrightarrow Li_xTiO_2 (0 \leqslant x \leqslant 1)$.

It is reported that rutile in its bulk crystalline form can only accommodate negligible Li (<0.1 Li per TiO_2 unit) at room temperature [17]. However, the lithium reactivity increases with decreasing the particle size because lithium storage on the surface of nanoparticles can be energetically more favorable than bulk insertion [18].

Mesoporous rutile TiO_2 nanoneedles prepared by the microemulsion-mediated sol–gel method at room temperature deliver initial discharge capacity of 305 mA h g^{-1} and sustains a capacity of 128 mA h g^{-1} beyond 15 cycles (Fig. 4). This improvement in cyclic performance is due to highly porous TiO_2 nanoneedles which accommodate the mechanical strains and shorten the length of lithium ion diffusion path. The first discharge curve shows three distinct regions (Fig. 4, inset) which is very similar to the reported results [11b]. For region I, the initial potential drops from OCV to about 1.45 V, corresponding to a storage of 0.16 Li, which is a common phenomenon linked to the decrease in particle and crystallite size for the nanometer-sized materials. For region II, a short plateau can be observed at 1.45 V corresponding to a storage of 0.53 Li. For region III, a second plateau can be observed at 1 V corresponding to storage of 0.22 Li. The first cycle shows a higher irreversible capacity loss of 139 mA h g^{-1}. However, a second cycle shows a lower irreversible capacity loss (20 mA h g^{-1}).

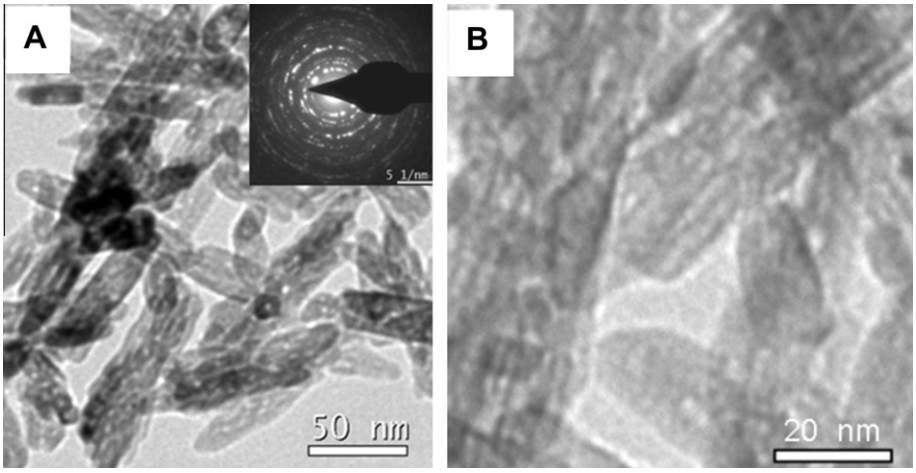

Fig. 2. (A and B) TEM images of as-synthesized mesoporous rutile TiO_2 nanoneedles. Inset in (A) shows corresponding SAED pattern.

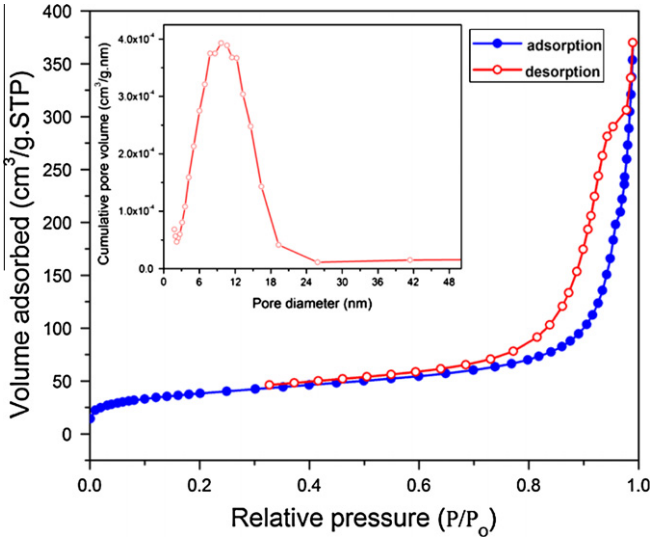

Fig. 3. N_2 adsorption–desorption isotherms and BJH pore-size distribution plot (inset) for as-synthesized rutile TiO_2 nanoneedles.

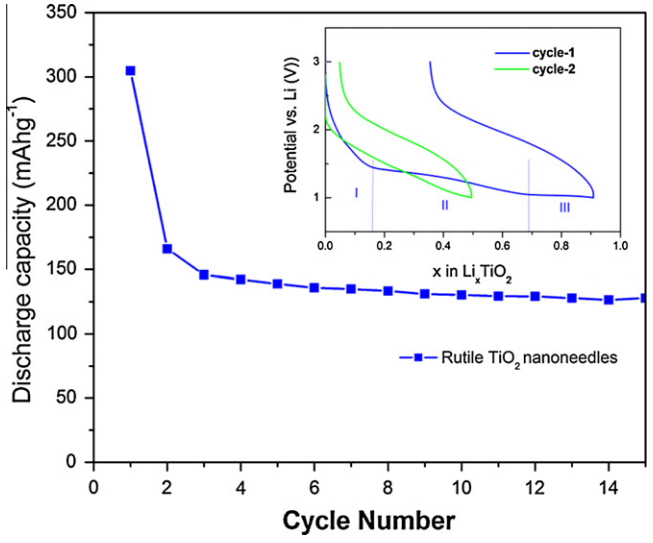

Fig. 4. Discharge capacity for mesoporous rutile TiO_2 nanoneedles prepared by the microemulsion-mediated sol–gel method at C/10 rate. Galvanostatic curve of TiO_2 rutile C/10 between 1 and 3 V vs Li^+/Li for the first and second cycle (inset).

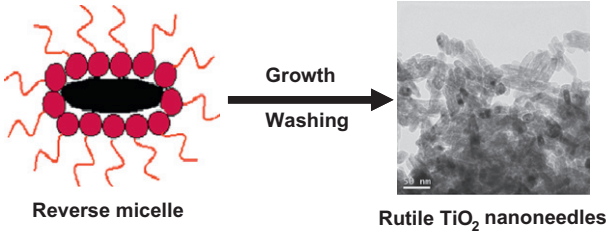

Fig. 5. Scheme for the formation of rutile TiO_2 nanoneedles in reverse micelle.

3.5. Mechanism for the formation of rutile TiO_2 nanoneedles in reverse microemulsion

Based on the experimental results, a possible growth mechanism for the formation of mesoporous rutile TiO_2 nanoneedles in a Triton X-100/cyclohexane/*n*-hexanol/water reverse micelle can be proposed. Triton X-100 is a well-defined nonionic (neutral) surfactant. Its structure contains a long hydrophilic poly(oxy-ethylene) chain terminated with the hydroxyl group. It forms nonspherical reverse micelles in cyclohexane [6c,19,20]. When titanium (IV) isopropoxide was slowly added to the reverse microemulsion, initially titanium (IV) isopropoxide was soluble in a continuous oil phase and after hydrolysis it forms water-soluble species that are situated within the elongated water droplets. The reverse micelle shows the formation of elongated nuclei, after the hydrolysis of the precursor. During the aging process, the growth of the nuclei takes place in one dimension only due to the constraint of the cylindrical shape of the micelles resulting in a nanoneedle mrophology (Fig. 5). This is my correlation analysis on the basis of experimental results; some detailed formation process of the mesoporous rutile TiO_2 nanoneedles still needs to be investigated further.

4. Conclusion

This communication presents a new, practical, and straightforward method for the preparation of rutile TiO_2 nanoneedles by a reverse microemulsion-mediated sol–gel method at room temperature. The basic principle of my approach is to produce highly uniform dispersions of nonspherical water droplets in an oil phase using Triton X-100 (more favorable to form nonspherical micelles) at room temperature and to spatially restrict the hydrolysis of alkoxide precursor within these nonspherical droplets (nanoreactors) which acts as a template to generate nanonedles. This is not

possible by the conventional sol–gel method. The prepared rutile TiO_2 powder, which has a needle-like mesoporous structure, showed a high specific surface area of 135 m^2/g compared to conventional sol–gel-derived materials. The rutile TiO_2 nanoneedles showed an initial discharge capacity of 305 mA h g^{-1} and sustain a capacity value of 128 mA h g^{-1} beyond 15 cycles. It is expected that this method can be generalized for synthesizing nanoneedles of other metal oxides after appropriate modifications.

Acknowledgments

I thank Dr. A.S. Prakash, Dr. K. Ramesha, and M. Sathiya for their help and cooperation. Financial support from Council of Scientific and Industrial Research (CSIR), New Delhi, India, is gratefully acknowledged.

References

[1] (a) Z.L. Wang, Adv. Mater. 12 (2000) 1295;
(b) J. Hu, T.W. Odom, C.M. Lieber, Acc. Chem. Res. 22 (1999) 435.
[2] Y. Xia, P. Yang, Y. Sun, et al., Adv. Mater. 15 (2003) 353.
[3] (a) A. Zhang, S.T. Aruna, S. Tirosh, B.A. Gregg, Y.J. Mastal, J. Phys. Chem. B 104 (2000) 4130;
(b) X. Zhang, G.H. Li, Y.X. Jin, Y. Zhang, J. Zhang, L.D. Zhang, Chem. Phys. Lett. 365 (2002) 300;
(c) Q. Zhang, L. Gao, Langmuir 19 (2003) 967.
[4] (a) C.-S. Kim, B.K. Moon, J.-H. Park, B.-C. Choi, H.-J. Seo, J. Cryst. Growth 257 (2003) 309;
(b) X.-L. Li, Q. Peng, J. -X Yi, X. Wang, Y. Li, Chem. Eur. J. 12 (2006) 2383.
[5] (a) B.B. Lakshmi, P.K. Dorhout, C.R. Martin, Chem. Mater. 9 (1997) 857;
(b) M. Zhang, Y. Bando, K. Wada, J. Mater. Sci. Lett. 20 (2001) 167.
[6] (a) Q. Limin, Encyclopedia of Surface and Colloid Science, 2006, p. 6183, doi:10.1081/E-ESCS-120023694;
(b) H. Shi, L. Qi, J. Ma, H. Cheng, Chem. Commun. (2002) 1704;
(c) P.K. Sahu, B.D. Kulkarni, R.B. Khomane, S.A. Pardhy, U.D. Phalgune, P. Rajmohanan, Renu Pasricha, Chem. Commun. (2003) 1876;
(d) X. Chen, S.S. Mao, Chem. Rev. 107 (2007) 2891.
[7] (a) M. Sander, M.J. Cote, W. Gu, B.M. Kile, C.P. Tripp, Adv. Mater. 16 (2004) 2052;
(b) A. Sadeghzadeh Attar, M. Sasani Ghamsari, F. Hajiesmaeilbaigi, Sh. Mirdamadi, K. Katagiri, K. Koumoto, J. Mater. Sci. 43 (2008) 5924.
[8] S. Brunauer, P.H. Emmett, E. Teller, J. Am. Chem. Soc. 60 (1938) 309.
[9] K.S.W. Sing, D.H. Everett, R.A.W. Haul, L. Moscou, R.A. Pierotti, J. Rouquerol, T. Siemieniewska, Pure Appl. Chem. 57 (1985) 603.
[10] (a) W. Ho, J.C. Yu, S. Lee, Chem. Commun. (2006) 1115;
(b) A.L. Linsebigler, G. Lu, J.T. Yates Jr., Chem. Rev. 95 (1995) 735;
(c) G.C. Li, Z.K. Zhang, Mater. Lett. 58 (2004) 2768.
[11] (a) D. Wang, D. Choi, Z. Yang, V.V. Viswanathan, Z. Nie, C. Wang, Y. Song, Ji-G Zhang, J. Liu, Chem. Mater. 20 (2008) 3435;
(b) P. Kubiak, M. Pfanzelt, J. Geserick, U. Hörmann, N. Hüsing, U. Kaiser, M. Wohlfahrt-Mehrens, J. Power Sources 194 (2009) 1099.
[12] (a) B. O'Regan, M. Gratzel, Nature 353 (1991) 737;
(b) H.S. Jung, J.K. Lee, M. Nastasi, S.W. Lee, J.Y. Kim, J.S. Park, K.S. Hong, H. Shin, Langmuir 21 (2005) 10332;
(c) S. Nakade, M. Matsuda, S. Kambe, Y. Saito, T. Kitamura, T. Sakata, Y. Wada, H. Mori, S. Yanagida, J. Phys. Chem. B 106 (2002) 10004.
[13] (a) Y. Zhu, J. Shi, Z. Zhang, C. Zhang, X. Zhang, Anal. Chem. 74 (2002) 120;
(b) N. Wu, S. Wang, I.A. Rusakova, Science 285 (1999) 1375.
[14] B. Zachau-Christiansen, K. West, T. Jacobsen, S. Atlung, Solid State Ionics 28 (1998) 1176.
[15] (a) D. Wang, D. Choi, Z. Yang, V.V. Viswanathan, Z. Nie, C. Wang, Y. Song, J.G. Zhang, J. Liu, Chem. Mater. 20 (2008) 3435;
(b) M.A. Reddy, M.S. Kishore, V. Pralong, V. Caignaert, U.V. Varadaraju, B. Raveau, Electrochem. Commun. 8 (2006) 1299.
[16] E.P. Barrett, L.G. Joyner, P.P. Halenda, J. Am. Chem. Soc. 73 (1951) 373.
[17] S. Takai, M. Kamata, S. Fujine, K. Yoneda, K. Kanda, T. Esaka, Solid State Ionics 123 (1999) 165.
[18] Y.-S. Hu, Kienle Lorenz, Y.-G. Guo, J. Maier, Adv. Mater. 18 (2006) 1421.
[19] D. Kuang, A. Xu, Y. Fang, H. Ou, H. Liu, J. Cryst. Growth 244 (2002) 379.
[20] W. Chen, Q. Zhu, Mater. Lett. 61 (2007) 3378.